Competing Vortex Topologies in Iron-Based Superconductors

Lun-Hui Hu,[1,2,3] Xianxin Wu,[4,5] Chao-Xing Liu,[3] and Rui-Xing Zhang[1,6,2,*]

[1]Department of Physics and Astronomy, The University of Tennessee, Knoxville, Tennessee 37996, USA
[2]Institute for Advanced Materials and Manufacturing, The University of Tennessee, Knoxville, Tennessee 37920, USA
[3]Department of Physics, The Pennsylvania State University, University Park, Pennsylvania 16802, USA
[4]CAS Key Laboratory of Theoretical Physics, Institute of Theoretical Physics, Chinese Academy of Sciences, Beijing 100190, China
[5]Max-Planck-Institut für Festkörperforschung, Heisenbergstrasse 1, D-70569 Stuttgart, Germany
[6]Department of Materials Science and Engineering, The University of Tennessee, Knoxville, Tennessee 37996, USA

(Received 3 November 2021; accepted 7 December 2022; published 29 December 2022)

In this Letter, we establish a new theoretical paradigm for vortex Majorana physics in the recently discovered topological iron-based superconductors (TFeSCs). While TFeSCs are widely accepted as an exemplar of topological insulators (TIs) with intrinsic *s*-wave superconductivity, our theory implies that such a common belief could be oversimplified. Our main finding is that the normal-state bulk Dirac nodes, usually ignored in TI-based vortex Majorana theories for TFeSCs, will play a key role of determining the vortex state topology. In particular, the interplay between TI and Dirac nodal bands will lead to multiple competing topological phases for a superconducting vortex line in TFeSCs, including an unprecedented hybrid topological vortex state that carries both Majorana bound states and a gapless dispersion. Remarkably, this exotic hybrid vortex phase generally exists in the vortex phase diagram for our minimal model for TFeSCs and is directly relevant to TFeSC candidates such as LiFeAs. When the fourfold rotation symmetry is broken by vortex-line tilting or curving, the hybrid vortex gets topologically trivialized and becomes Majorana free, which could explain the puzzle of ubiquitous trivial vortices observed in LiFeAs. The origin of the Majorana signal in other TFeSC candidates such as $FeTe_xSe_{1-x}$ and $CaKFe_4As_4$ is also interpreted within our theory framework. Our theory sheds new light on theoretically understanding and experimentally engineering Majorana physics in high-temperature iron-based systems.

DOI: 10.1103/PhysRevLett.129.277001

Introduction.—The inherent resilience of a topological quantum computer (TQC) makes it one of the most promising paradigms for processing information in a fully quantum mechanical manner [1–4]. This inspiring concept of TQC has motivated an intensive experimental search for Majorana zero modes [5–22], the simplest and most feasible building block for TQCs. While a "smoking gun" for Majorana modes is still lacking, the recent advent of topological iron-based superconductors [23–34] (TFeSCs) sheds light on resolving this long-sought Majorana mystery [35–49]. Remarkably, the normal-state band structure of TFeSCs naturally contains two crucial ingredients: (i) a topological insulator (TI) part that provides a helical Dirac surface state [50–52] and (ii) cylindrical Fermi surfaces that generate intrinsic bulk superconductivity [53–61], which together resemble the well-known Majorana paradigm proposed by Fu and Kane [62]. Indeed, strong evidence of field-induced vortex Majorana bound states (VMBSs) has been observed in multiple iron-based systems [29–34].

The TFeSCs, however, are far from being well understood. For example, unlike other TFeSC candidates, LiFeAs possesses no VMBS signal in any of its free vortices, even though the Fermi level is around the TI gap [34]. This counter-intuitive vortex physics clearly deviates from the naive expectation from the Fu-Kane paradigm, thus calling for a new theoretical interpretation. Meanwhile, most TFeSCs additionally host a pair of massless bulk Dirac nodes in their normal states [25,63], which are energetically above the TI bands with an energy separation dubbed δ_{so}. It has been predicted that a Dirac semimetal (DSM), if going superconducting, would feature gapless, VMBS-free magnetic vortices [64,65], in contrast to the VMBS physics of a superconducting TI [62,66–74]. Notably, existing studies on TFeSCs generally adopt the presumption of an infinite δ_{so} limit, so that only TI or DSM bands are independently studied for simplicity [75]. However, such presumption remains unjustified for some TFeSC candidates (e.g., LiFeAs) where δ_{so} can be as small as 10 meV [25,76]. This raises an important open question for the topological nature of vortices in TFeSCs, especially when both TI and DSM bands are highly entangled.

In this Letter, we provide a new theoretical paradigm for understanding vortex topological physics in general TFeSCs. To fully incorporate both TI and DSM physics, a minimal six-band model is constructed to capture the key topological ingredients of general TFeSCs [25,51]. For the

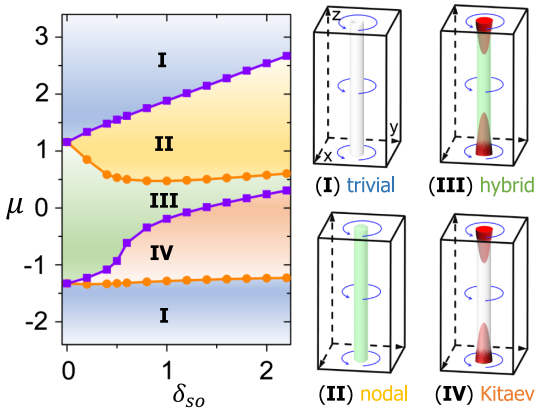

FIG. 1. The vortex topological phase diagram for a minimal TFeSC model is mapped out as a function of chemical potential μ and $\delta_{\rm so}$, the separation energy between the TI gap and bulk Dirac nodes. It contains four phases: (I) trivial vortex; (II) nodal vortex; (III) hybrid vortex with both 0D end-localized VMBSs (red cone) and 1D gapless channels. (IV) Kitaev vortex with 0D end-localized VMBSs.

first time, we have identified the emergence of four competing and topologically distinct vortex states in the vortex phase diagram of TFeSCs, as shown in Fig. 1. Remarkably, a new exotic "hybrid topological" vortex phase manifests as the most probable vortex state for small $\delta_{\rm so}$ systems, which features both well-defined VMBS and a one-dimensional (1D) nodal band structure along its k_z dispersion. The stability of the hybrid vortex phase relies on the protection of four-fold rotation symmetry C_4, and upon C_4 breaking, the hybrid vortex can be easily trivialized to become VMBS free. This offers a natural explanation for the observed missing-Majorana puzzle in LiFeAs [34]. Applications of our theory to other TFeSCs and new experimental signatures are also discussed.

Model Hamiltonian.—We start by defining a minimal $\mathbf{k}\cdot\mathbf{p}$ Hamiltonian that captures the key low-energy topological physics of general TFeSCs [25,51]. We first consider a normal-state basis $\Psi_{\mathbf{k}} = (|p_z,\uparrow\rangle, |p_z,\downarrow\rangle, |d_{xz+iyz},\downarrow\rangle, |d_{xz-iyz},\uparrow\rangle, |d_{xz+iyz},\uparrow\rangle, |d_{xz-iyz},\downarrow\rangle)^T$, which, in the angular momentum basis, becomes $\Psi_{\mathbf{k}} = (|p_-,\frac{1}{2}\rangle, |p_-,-\frac{1}{2}\rangle, |d_+,\frac{1}{2}\rangle, |d_+,-\frac{1}{2}\rangle, |d_+,\frac{3}{2}\rangle, |d_+,-\frac{3}{2}\rangle)^T$. Here, $|\alpha_\eta, J_z\rangle$ denote a basis originating from $\alpha = p,\ d$ atomic orbitals that carries both a z-component angular momentum J_z and a parity index $\eta = \pm$. Then the normal-state Hamiltonian is

$$\mathcal{H}_0(\mathbf{k}) = \begin{pmatrix} h^{(\frac{1}{2})}(\mathbf{k}) & T(\mathbf{k}) \\ T^\dagger(\mathbf{k}) & h^{(\frac{3}{2})}(\mathbf{k}) \end{pmatrix} \tag{1}$$

which consists of $h^{\frac{3}{2}}(\mathbf{k}) = [M_2(\mathbf{k}) + \delta_{\rm so}]\sigma_0$ and

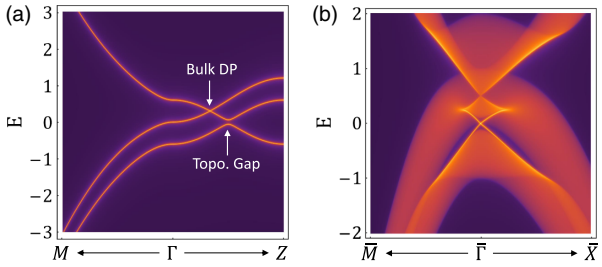

FIG. 2. Bulk and (001) surface energy spectra are shown in (a) and (b), respectively. Both TI and DSM physics coexist and are energetically separated by an energy scale of $\delta_{\rm so}$.

$$h^{(\frac{1}{2})}(\mathbf{k}) = \begin{pmatrix} M_1(\mathbf{k}) & 0 & A_2k_z & -A_1k_- \\ 0 & M_1(\mathbf{k}) & A_1k_+ & A_2k_z \\ A_2k_z & A_1k_- & M_2(\mathbf{k}) & 0 \\ -A_1k_+ & A_2k_z & 0 & M_2(\mathbf{k}) \end{pmatrix}$$
$$T^\dagger(\mathbf{k}) = \begin{pmatrix} A_1k_- & 0 & 0 & D^*(\mathbf{k}) \\ 0 & -A_1k_+ & D(\mathbf{k}) & 0 \end{pmatrix}. \tag{2}$$

Here σ denotes the Pauli matrix for spin degree of freedom, and we have defined $k_\pm = k_x \pm ik_y$, $M_i(\mathbf{k}) = M_0^{(i)} + M_1^{(i)}(k_x^2+k_y^2) + M_2^{(i)}k_z^2$ and $D(\mathbf{k}) = D_1(k_x^2-k_y^2) - iD_2k_xk_y$. $H_0(\mathbf{k})$ features fourfold rotation symmetry $C_4 = e^{i(\pi/2)J_z}$, inversion symmetry $\mathcal{P} = \mathrm{diag}[-1,-1,1,1,1,1]$, and time-reversal symmetry $\Theta = \mathrm{diag}[-i,i,-i]\otimes\sigma_y\mathcal{K}$, with $J_z = \mathrm{diag}[\frac{1}{2},-\frac{1}{2},\frac{1}{2},-\frac{1}{2},\frac{3}{2},-\frac{3}{2}]$ and $\mathcal{K}$ denoting the complex conjugation operation. For our purpose, we choose $M_0^{(1)} = M_1^{(1)} = -2M_2^{(1)} = -1$, $A_1 = 0.5$, $A_2 = 0.1$, $D_{1,2} = 0$ and $M_{0,1,2}^{(2)} = -M_{0,1,2}^{(1)}$ throughout this Letter. This ensures an inverted band structure among the p_z and $d_{xz,yz}$ bands.

Notably, $h^{(\frac{1}{2})}(\mathbf{k})$ by itself manifests as a standard Hamiltonian for a 3D time-reversal invariant TI [77,78]. In addition, as shown in Fig. 2(a), a second band inversion between $|p_-,\pm\frac{1}{2}\rangle$ and $|d_+,\pm\frac{3}{2}\rangle$ generates an additional 3D Dirac semimetal phase with a pair of fourfold-degenerate bulk Dirac nodes [79,80]. The energy separation between the TI and DSM bands is controlled by $\delta_{\rm so}$, the spin-orbit splitting among the d-orbital bands. Remarkably, the robustness of the bulk Dirac points are guaranteed by the combination of C_4, $\mathcal{P}$, and Θ. In Fig. 2(b), we exploit the iterative Green function method to map out the energy spectrum for (001) surface in a semi-infinite geometry. This clearly reveals the coexistence of a 2D Dirac surface state and the 3D bulk Dirac nodes, a common topological feature shared by most TFeSCs.

Kitaev, nodal, and hybrid topological vortices.—When the system becomes superconducting, the corresponding Bogoliubov-de Gennes (BdG) Hamiltonian is

$$\mathcal{H}_{BdG} = \begin{pmatrix} \mathcal{H}_0(\mathbf{r}) & \mathcal{H}_\Delta \\ \mathcal{H}_\Delta^\dagger & -\mathcal{H}_0^*(\mathbf{r}) \end{pmatrix}, \tag{3}$$

under the Nambu basis $\{\Psi_{\mathbf{r}}^{\dagger}, \Psi_{\mathbf{r}}^{T}\}$. We consider an isotropic s-wave pairing Hamiltonian $\mathcal{H}_{\Delta} = i\Delta(\mathbf{r})\mathrm{diag}[1,-1,1] \otimes \sigma_y$ [81]. A single magnetic vortex line can be described by $\Delta(\mathbf{r}) = \Delta_0 \tanh(r/\xi_0)e^{i\theta}$, where $\Delta_0 = 0.2$, (r,θ) are the in plane polar coordinates with respect to the vortex core and ξ_0 denotes the superconducting coherence length. Physically, a vortex line is a 1D class D system [83], which, if being gapped, admits a Z_2 band topology that determines the presence of VMBS.

To understand possible vortex topologies in TFeSCs, it is suggestive to start with a $\delta_{\mathrm{so}} \to \infty$ limit, where the normal-state TI phase and DSM phase can be viewed as two independent systems [75]. When the Fermi level lies around the TI gap, the system enters the "TI limit," and its vortex physics is well captured by the Fu-Kane model [62,66]. Specifically, the lowest-energy k_z-dispersing vortex-line modes carry an angular momentum of $l_z = 0$, and there exist two critical chemical potentials $\mu = \mu_{c0,\pm}$ where the vortex modes close their energy gap at $k_z = 0$ or π. Such gap closing signals a change of the 1D vortex topology and thus serves as the phase boundaries for two topologically distinct phases: (i) a Majorana-free trivial phase and (ii) a gapped topological phase with end-localized VMBS (dubbed the "Kitaev vortex"), which lives within $\mu \in (\mu_{c0,-}, \mu_{c0,+})$.

Meanwhile, a "DSM limit" with $\delta_{\mathrm{so}} \to \infty$ is reached when the Fermi level is near the bulk Dirac nodes. Similarly, there exist two critical chemical potentials $\mu_{c1,\pm}$ where the vortex gap vanishes at $k_z = 0$ or π. For $\mu \in (\mu_{c1,-}, \mu_{c1,+})$, however, the lowest-energy vortex modes necessarily carry $l_z = \pm 1$ and further form a pair of C_4-protected band crossings at zero energy along k_z. While such a nodal vortex is NOT VMBS carrying, it can be turned into a gapped Kitaev vortex with VMBS by simply spoiling the protecting C_4 symmetry, as we will show later.

In realistic FeSC systems, δ_{so} can be small enough such that neither the TI limit nor the DSM limit applies. In this case, the aforementioned phase diagrams for both TI and DSM limits will now mix and interact with each other. Nonetheless, the notions of $\mu_{c0,\pm}$ and $\mu_{c1,\pm}$ remain well defined and thus still decide the vortex topological phase boundaries even for a small δ_{so} system. Remarkably, as we show analytically in the Supplemental Material [84], the energy range for each vortex phase, i.e., $\Delta\mu_{c0/c1} = \mu_{c0/c1,+} - \mu_{c0/c1,-}$, will get significantly enhanced by reducing the value of δ_{so}. This fact is crucial for small-δ_{so} systems, where the Kitaev vortex phase and nodal vortex phase tend to have a finite overlap around $\mu = 0$ in the phase diagram, leading to a new *hybrid topological vortex phase*. This hybrid vortex state inherits two key topological features from its parent vortex states: (i) it features a C_4-protected nodal dispersion along k_z and (ii) it hosts VMBS with a finite localization length. Notably, the 1D nodal bands and the VMBSs are living in different C_4 symmetry sectors and thus will not hybridize with each other. A similar Majorana-carrying gapless topological phase has also been reported in certain 1D Luttinger-liquid systems [93,94].

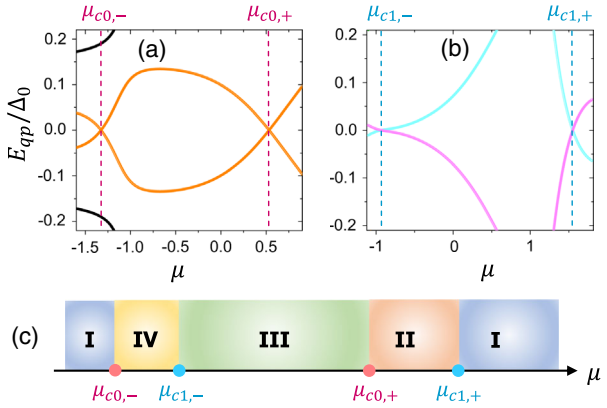

FIG. 3. The 1D vortex spectrum at $k_z = \pi$ is shown in (a) for $l_z = 0$ and (b) for $|l_z| = 1$. All the other subspaces with $|l_z| > 1$ are fully gapped. The critical chemical potentials, with which the energy gap closes, determine the phase boundaries for the vortex phase diagram schematically shown in (c).

We now proceed to numerically map out the vortex topological phase diagram (VTPD) for our six-band TFeSC model in Eq. (3) as a function of both μ and δ_{so}. The topological phase boundaries in Fig. 1 are determined by $\mu_{c0,\pm}$ (orange line) and $\mu_{c1,\pm}$ (purple line) for a fixed δ_{so}, which can be extracted by calculating the vortex mode spectrum. We therefore consider a cylindrical geometry [95] for our TFeSC model, with k_z being a good quantum number and open boundary conditions imposed for in plane directions. Details of numerical calculations are discussed in the Supplemental Material [84]. As shown in Figs. 3(a) and 3(b), we plot the vortex mode spectrum as a function of μ with fixed $\delta_{\mathrm{so}} = 0.5$ and $k_z = \pi$ for both $l_z = 0$ and $|l_z| = 1$ sectors, respectively, where the gap closing points indicate the topological phase boundaries as defined in the insets. The vortex spectra with $|l_z| \geq 2$ are fully gapped. Four topologically inequivalent regions are found to show up, as shown in Fig. 3(c): (I) trivial vortex for either $\mu > \mu_{c1,+}$ or $\mu < \mu_{c0,-}$; (II) nodal vortex for $\mu_{c0,+} < \mu < \mu_{c1,+}$; (III) hybrid vortex for $\mu_{c1,-} < \mu < \mu_{c0,+}$; (IV) Kitaev vortex for $\mu_{c0,-} < \mu < \mu_{c1,-}$. Further varying the value of δ_{so}, we eventually obtain the complete μ-δ_{so} VTPD in Fig. 1. Just as we expect, the hybrid vortex is indeed the dominating phase for clean TFeSCs with small μ and δ_{so}.

The hybrid vortex physics is captured by a minimal four-band effective Hamiltonian,

$$h_{\mathrm{hybrid}}(k_z) = h_{\mathrm{Kitaev}}(k_z) \oplus h_{\mathrm{nodal}}(k_z). \tag{4}$$

The decoupled 2×2 blocks $h_{\mathrm{Kitaev}} = (m_0 + m_1 k_z^2)\tau_z + m_2 k_z \tau_x$ and $h_{\mathrm{nodal}} = (m_0' + m_1' k_z^2)\tau_z$ correspond to the

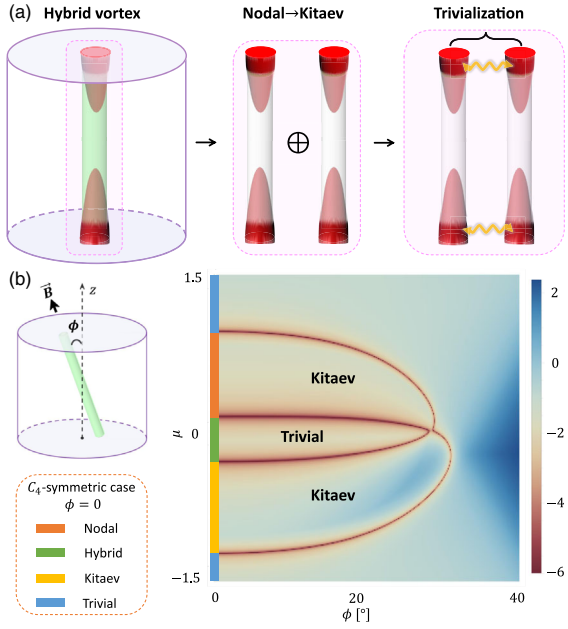

FIG. 4. (a) Vortex-line tilting gaps out the nodal componenet of a hybrid vortex, leading to two copies of Kitaev vortex states that can be trivialized topologically together. (b) The vortex topological phase diagram as a function of μ and ϕ for $\delta_{\rm so} = 0.5$. The logarithmic value of the vortex energy gap at $k_z' = \pi$ is shown by the colors. The red lines denote vortex topological phase transitions.

gapped Kitaev vortex part with $l_z = 0$ and the gapless nodal vortex part with $l_z = \pm 1$, respectively. While it can be easily constructed with the symmetry principle, we also provide an analytical derivation of $h_{\rm hybrid}$ in the Supplemental Material [84]. The band parameters for $h_{\rm hybrid}$ can be extracted numerically. For example, with $\mu = 0$, $\delta_{\rm so} = 0.5$, we find $m_0 = 0.018$, $m_1 = -0.0022$, $m_2 = 0.032$ and $m_0' = 0.025$, $m_1' = -0.011$ for the above model. The fact that $m_0 m_1 < 0$ and $m_0 m_1 < 0$ signals the topological band inversions for both $h_{\rm Kitaev}$ and $h_{\rm nodal}$.

The topological nature of the hybrid vortex state delicately relies on the around-axis C_4 symmetry. As schematically shown in Fig. 4(a), spoiling C_4 drives the nodal component of the hybrid vortex into additional Kitaev vortex degrees of freedom, which further interacts with the original Kitaev vortex component and gets trivialized as a whole. Therefore, a C_4-broken "hybrid vortex" is essentially a trivial vortex state with no Majorana physics. In practice, local C_4 breaking at the nanometer scale appears generally unavoidable and can arise from a plethora of mechanisms in TFeSCs. These scenarios include (i) the applied magnetic field tilting away from the $\hat{z}$ axis [85,96,97] and (ii) bulk impurities bending the vortex line. In the following, we will focus on the effect of vortex-line tilting in TFeSCs and a detailed discussion of the vortex-line bending can be found in the Supplemental Material [84].

Vortex-line tilting.—For a small tilting angle $\phi \ll (\pi/2)$ [as defined in Fig. 4(b)], we can adopt the second-order perturbation theory to analytically rederive the hybrid vortex Hamiltonian $h_\phi(k_z')$, where k_z' is aligned with the vortex-line orientation. Details of the perturbation theory can be found in the Supplemental Material [84]. We find that formally,

$$h_\phi(k_z') = h_{\rm hybrid}(k_z', \phi) + h_{\rm SB}(k_z', \phi) + \mathcal{O}(\phi^3). \quad (5)$$

Here $h_{\rm hybrid}(k_z', \phi)$ resembles the original C_4-preserving hybrid vortex Hamiltonian in Eq. (4), but with a set of renormalized parameters $m_{0,1} \to m_{0,1} + m_{5,6}\phi^2$ and $m_{0,1}' \to m_{0,1}' + m_{5,6}'\phi^2$. We thus expect turning on ϕ to quantitatively change our VTPD (i.e., $\mu_{c0,\pm}$ and $\mu_{c1,\pm}$).

Meanwhile, $h_{\rm SB}(k_z', \phi)$ describes the geometry-induced C_4 breaking terms, and its effects on the vortex-state topology are twofold. First, it generates a topological gap for the nodal vortex bands, with $h_{\rm nodal} \to h_{\rm nodal} + m_2'\phi^2 k_z' \tau_x$. The linear-$k_z$ dependence here is required by the particle-hole symmetry $\Xi = \tau_x \mathcal{K}$, with $\mathcal{K}$ the complex conjugation. Second, the Kitaev and nodal vortex degrees of freedom get hybridized via a coupling matrix that is linearly proportional to ϕ (see the Supplemental Material [84] for details). Therefore, it is exactly the above two contributions of $h_{\rm SB}(k_z', \phi)$ that lead to the "hybrid → trivial" scenario described in Fig. 4(a).

Figure 4(b) is a numerical map of VTPD as a function of μ and ϕ based on a lattice-regularized tight-binding model of Eq. (3), by calculating the logarithmic value of the vortex band gap at $k_z' = \pi$. In the $\phi = 0$ limit, the μ-ϕ VTPD reproduces the C_4-symmetric phase diagram in Fig. 3(c), up to some quantitative differences from the lattice regularization procedure. The topological vortex phase boundaries (red lines) manifest a ϕ dependence due to the vortex band renormalization, agreeing with our perturbation theory. Interestingly, we also find that the Kitaev vortex phase will terminate at $\phi \sim \pi/6$, which can be easily checked in experiments by mapping out the local density of states near the vortex core.

Discussions on TFeSCs candidates.—We first note that $FeTe_xSe_{1-x}$, a paradigmatic TFeSC candidate, features a strong spin-orbital coupling effect with $\delta_{\rm so} \sim 35$ meV. We believe that such $\delta_{\rm so}$ is large enough for $FeTe_xSe_{1-x}$ to approach the "TI limit," as justified by earlier first-principles-based calculations [51]. Thus, $FeTe_xSe_{1-x}$ should manifest as a standard Fu-Kane superconductor with VMBS signals, agreeing with the experimental observations [23,29].

LiFeAs, however, features a small $\delta_{\rm so} \sim 10.7$ meV [25], three times smaller than that of $FeTe_xSe_{1-x}$. Based on the μ-$\delta_{\rm so}$ VTPD in Fig. 1, we expect LiFeAs to carry the hybrid vortex topology for hosting both small $\delta_{\rm so}$ and μ. As we discussed earlier, a C_4-breaking perturbation such as the **B** field tilting in Fig. 4 can break the hybrid vortex down to a

trivial one with no VMBS signal, which is likely the reason behind the disappearance of vortex Majorana signals in LiFeAs [34]. In particular, even when the **B** field is carefully aligned with the crystalline rotation axis, the tilting angle ϕ of the vortex line can still be greatly enhanced, when a near-surface impurity locally distorts the vortex-line geometry. Notably, these atomic impurities could be completely invisible to surface-sensitive probes, such as scanning tunneling microscopy. In the Supplemental Material [84], we numerically simulate such an impurity-induced vortex-line bending effect and have confirmed its crucial role of trivializing vortex topology.

Reference [34] also reports the appearance of a VMBS signal in LiFeAs due to surface-impurity-induced electron doping. The reported levitation of the Fermi level is around 5 meV for the so-called strong impurities. Given that $\delta_{so} \sim 10$ meV for LiFeAs, this effect would be capable of driving a transition from a trivialized hybrid vortex to a Kitaev vortex, following our μ-ϕ VTPD in Fig. 4(b). We further predict that if we continuously lower the Fermi level via hole doping, *the VMBS signal will reemerge at a critical* $\mu_{c1,-}$ [i.e., regime IV in Fig. 3(c)] *and eventually disappear at a negatively large* $\mu_{c0,-}$. Such an exotic "reentrant Majorana signal" serves as an experimental "smoking gun" for our theory. We also predict a similar but more complex reentrant vortex Majorana phenomenon in $CaKFe_4As_4$ [33], where a detailed discussion can be found in the Supplemental Material [84].

Conclusion.—To summarize, the entanglement between TI and DSM physics has a decisive impact on the topological nature of vortex lines in TFeSCs. A direct outcome of the entangled bulk topological bands is the competition among multiple topologically distinct vortex states in the VTPD, including trivial, Kitaev, nodal, and hybrid vortex phases. Notably, the unprecendented hybrid vortex topology naturally explains the puzzling absence of a VMBS signal in LiFeAs. Our theory can also be feasibly tested in both LiFeAs and $CaKFe_4As_4$ with the state-of-the-art Fermi level engineering and scanning tunneling microscopy. In addition, by replacing the Te/Se/As atoms in TFeSCs with other atoms with different spin-orbital coupling, the value of δ_{so} can be continuously tuned to manipulate the vortex topology. An interesting future direction is to explore other symmetry breaking effects and their impact on the vortex topology in TFeSCs. For example, breaking inversion symmetry by strain can split the bulk Dirac nodes into pairs of Weyl nodes, which is expected to further complicate the VTPD [71,96,97]. We leave a detailed study on these possibilities of engineering vortex topological physics to future works.

We acknowledge S. Das Sarma, C.-K. Chiu, and especially L. Kong for helpful discussions. C. X. L. acknowledges the support of the Office of Naval Research (Grant No. N00014-18-1-2793) and Kaufman New Initiative research (Grant No. KA2018-98553) of the Pittsburgh Foundation. L.-H. H. and R.-X. Z. acknowledge support from the start-up fund at the University of Tennessee.

Note added.—After the submission of our manuscript, we became aware of two experimental papers that reported a strain-induced hole-doping effect achieved in LiFeAs [98,99], where the reappearance of vortex-bound zero-bias peak signals is also found. These observations agree with our "reentrant Majorana signal" prediction.

*ruixing@utk.edu

[1] A. Y. Kitaev, Ann. Phys. (Amsterdam) **303**, 2 (2003).
[2] C. Nayak, S. H. Simon, A. Stern, M. Freedman, and S. Das Sarma, Rev. Mod. Phys. **80**, 1083 (2008).
[3] S. D. Sarma, M. Freedman, and C. Nayak, npj Quantum Inf. **1**, 15001 (2015).
[4] S. R. Elliott and M. Franz, Rev. Mod. Phys. **87**, 137 (2015).
[5] V. Mourik, K. Zuo, S. M. Frolov, S. Plissard, E. P. Bakkers, and L. P. Kouwenhoven, Science **336**, 1003 (2012).
[6] L. P. Rokhinson, X. Liu, and J. K. Furdyna, Nat. Phys. **8**, 795 (2012).
[7] J. R. Williams, A. J. Bestwick, P. Gallagher, S. S. Hong, Y. Cui, A. S. Bleich, J. G. Analytis, I. R. Fisher, and D. Goldhaber-Gordon, Phys. Rev. Lett. **109**, 056803 (2012).
[8] A. Das, Y. Ronen, Y. Most, Y. Oreg, M. Heiblum, and H. Shtrikman, Nat. Phys. **8**, 887 (2012).
[9] M. Deng, C. Yu, G. Huang, M. Larsson, P. Caroff, and H. Xu, Nano Lett. **12**, 6414 (2012).
[10] A. D. K. Finck, D. J. Van Harlingen, P. K. Mohseni, K. Jung, and X. Li, Phys. Rev. Lett. **110**, 126406 (2013).
[11] E. J. Lee, X. Jiang, M. Houzet, R. Aguado, C. M. Lieber, and S. De Franceschi, Nat. Nanotechnol. **9**, 79 (2014).
[12] S. Nadj-Perge, I. K. Drozdov, J. Li, H. Chen, S. Jeon, J. Seo, A. H. MacDonald, B. A. Bernevig, and A. Yazdani, Science **346**, 602 (2014).
[13] J.-P. Xu, M.-X. Wang, Z. L. Liu, J.-F. Ge, X. Yang, C. Liu, Z. A. Xu, D. Guan, C. L. Gao, D. Qian, Y. Liu, Q.-H. Wang, F.-C. Zhang, Q.-K. Xue, and J.-F. Jia, Phys. Rev. Lett. **114**, 017001 (2015).
[14] S. M. Albrecht, A. P. Higginbotham, M. Madsen, F. Kuemmeth, T. S. Jespersen, J. Nygård, P. Krogstrup, and C. Marcus, Nature (London) **531**, 206 (2016).
[15] H.-H. Sun, K.-W. Zhang, L.-H. Hu, C. Li, G.-Y. Wang, H.-Y. Ma, Z.-A. Xu, C.-L. Gao, D.-D. Guan, Y.-Y. Li, C. Liu, D. Qian, Y. Zhou, L. Fu, S.-C. Li, F.-C. Zhang, and J.-F. Jia, Phys. Rev. Lett. **116**, 257003 (2016).
[16] M. Deng, S. Vaitiekėnas, E. B. Hansen, J. Danon, M. Leijnse, K. Flensberg, J. Nygård, P. Krogstrup, and C. M. Marcus, Science **354**, 1557 (2016).
[17] Y.-F. Lv, W.-L. Wang, Y.-M. Zhang, H. Ding, W. Li, L. Wang, K. He, C.-L. Song, X.-C. Ma, and Q.-K. Xue, Sci. Bull. **62**, 852 (2017).
[18] B. E. Feldman, M. T. Randeria, J. Li, S. Jeon, Y. Xie, Z. Wang, I. K. Drozdov, B. A. Bernevig, and A. Yazdani, Nat. Phys. **13**, 286 (2017).

[19] S. Jeon, Y. Xie, J. Li, Z. Wang, B. A. Bernevig, and A. Yazdani, Science **358**, 772 (2017).

[20] H. Ren, F. Pientka, S. Hart, A. T. Pierce, M. Kosowsky, L. Lunczer, R. Schlereth, B. Scharf, E. M. Hankiewicz, L. W. Molenkamp *et al.*, Nature (London) **569**, 93 (2019).

[21] B. Jäck, Y. Xie, J. Li, S. Jeon, B. A. Bernevig, and A. Yazdani, Science **364**, 1255 (2019).

[22] A. Fornieri, A. M. Whiticar, F. Setiawan, E. Portolés, A. C. Drachmann, A. Keselman, S. Gronin, C. Thomas, T. Wang, R. Kallaher *et al.*, Nature (London) **569**, 89 (2019).

[23] P. Zhang, K. Yaji, T. Hashimoto, Y. Ota, T. Kondo, K. Okazaki, Z. Wang, J. Wen, G. Gu, H. Ding *et al.*, Science **360**, 182 (2018).

[24] X. Shi, Z.-Q. Han, P. Richard, X.-X. Wu, X.-L. Peng, T. Qian, S.-C. Wang, J.-P. Hu, Y.-J. Sun, and H. Ding, Sci. Bull. **62**, 503 (2017).

[25] P. Zhang, Z. Wang, X. Wu, K. Yaji, Y. Ishida, Y. Kohama, G. Dai, Y. Sun, C. Bareille, K. Kuroda *et al.*, Nat. Phys. **15**, 41 (2019).

[26] X.-L. Peng, Y. Li, X.-X. Wu, H.-B. Deng, X. Shi, W.-H. Fan, M. Li, Y.-B. Huang, T. Qian, P. Richard, J.-P. Hu, S.-H. Pan, H.-Q. Mao, Y.-J. Sun, and H. Ding, Phys. Rev. B **100**, 155134 (2019).

[27] L. Kong, S. Zhu, M. Papaj, H. Chen, L. Cao, H. Isobe, Y. Xing, W. Liu, D. Wang, P. Fan *et al.*, Nat. Phys. **15**, 1181 (2019).

[28] S. Zhu, L. Kong, L. Cao, H. Chen, M. Papaj, S. Du, Y. Xing, W. Liu, D. Wang, C. Shen *et al.*, Science **367**, 189 (2020).

[29] D. Wang, L. Kong, P. Fan, H. Chen, S. Zhu, W. Liu, L. Cao, Y. Sun, S. Du, J. Schneeloch *et al.*, Science **362**, 333 (2018).

[30] T. Machida, Y. Sun, S. Pyon, S. Takeda, Y. Kohsaka, T. Hanaguri, T. Sasagawa, and T. Tamegai, Nat. Mater. **18**, 811 (2019).

[31] Q. Liu, C. Chen, T. Zhang, R. Peng, Y.-J. Yan, C.-H.-P. Wen, X. Lou, Y.-L. Huang, J.-P. Tian, X.-L. Dong, G.-W. Wang, W.-C. Bao, Q.-H. Wang, Z.-P. Yin, Z.-X. Zhao, and D.-L. Feng, Phys. Rev. X **8**, 041056 (2018).

[32] C. Chen, Q. Liu, T. Zhang, D. Li, P. Shen, X. Dong, Z.-X. Zhao, T. Zhang, and D. Feng, Chin. Phys. Lett. **36**, 057403 (2019).

[33] W. Liu, L. Cao, S. Zhu, L. Kong, G. Wang, M. Papaj, P. Zhang, Y.-B. Liu, H. Chen, G. Li *et al.*, Nat. Commun. **11**, 1 (2020).

[34] L. Kong, L. Cao, S. Zhu, M. Papaj, G. Dai, G. Li, P. Fan, W. Liu, F. Yang, X. Wang *et al.*, Nat. Commun. **12**, 1 (2021).

[35] R.-X. Zhang, W. S. Cole, and S. Das Sarma, Phys. Rev. Lett. **122**, 187001 (2019).

[36] R.-X. Zhang, W. S. Cole, X. Wu, and S. Das Sarma, Phys. Rev. Lett. **123**, 167001 (2019).

[37] Z. Yan, F. Song, and Z. Wang, Phys. Rev. Lett. **121**, 096803 (2018).

[38] Q. Wang, C.-C. Liu, Y.-M. Lu, and F. Zhang, Phys. Rev. Lett. **121**, 186801 (2018).

[39] L.-H. Hu, C.-X. Liu, and F.-C. Zhang, Commun. Phys. **2**, 25 (2019).

[40] T. Kawakami and M. Sato, Phys. Rev. B **100**, 094520 (2019).

[41] X. Wu, X. Liu, R. Thomale, and C.-X. Liu, Natl. Sci. Rev. **9**, nwab087 (2022), nwab087.

[42] X. Wu, W. A. Benalcazar, Y. Li, R. Thomale, C.-X. Liu, and J. Hu, Phys. Rev. X **10**, 041014 (2020).

[43] M. J. Gray, J. Freudenstein, S. Y. F. Zhao, R. O' Connor, S. Jenkins, N. Kumar, M. Hoek, A. Kopec, S. Huh, T. Taniguchi *et al.*, Nano Lett. **19**, 4890 (2019).

[44] X. Wu, R.-X. Zhang, G. Xu, J. Hu, and C.-X. Liu, In the pursuit of majorana modes in iron-based high-t_c superconductors, in *Memorial Volume for Shoucheng Zhang* (World Scientific, 2021), Chap. 3, pp. 35–60.

[45] R.-X. Zhang and S. Das Sarma, Phys. Rev. Lett. **126**, 137001 (2021).

[46] M. Kheirkhah, Z. Yan, and F. Marsiglio, Phys. Rev. B **103**, L140502 (2021).

[47] S. Qin, C. Fang, F.-C. Zhang, and J. Hu, Phys. Rev. X **12**, 011030 (2022).

[48] M. Kheirkhah, Z.-Y. Zhuang, J. Maciejko, and Z. Yan, Phys. Rev. B **105**, 014509 (2022).

[49] T. Barik and J. D. Sau, Phys. Rev. B **105**, 035128 (2022).

[50] Z. Wang, P. Zhang, G. Xu, L. K. Zeng, H. Miao, X. Xu, T. Qian, H. Weng, P. Richard, A. V. Fedorov, H. Ding, X. Dai, and Z. Fang, Phys. Rev. B **92**, 115119 (2015).

[51] G. Xu, B. Lian, P. Tang, X.-L. Qi, and S.-C. Zhang, Phys. Rev. Lett. **117**, 047001 (2016).

[52] X. Wu, S. Qin, Y. Liang, H. Fan, and J. Hu, Phys. Rev. B **93**, 115129 (2016).

[53] Y. Kamihara, T. Watanabe, M. Hirano, and H. Hosono, J. Am. Chem. Soc. **130**, 3296 (2008).

[54] M. H. Fang, H. M. Pham, B. Qian, T. J. Liu, E. K. Vehstedt, Y. Liu, L. Spinu, and Z. Q. Mao, Phys. Rev. B **78**, 224503 (2008).

[55] T. Hanaguri, S. Niitaka, K. Kuroki, and H. Takagi, Science **328**, 474 (2010).

[56] J. Paglione and R. L. Greene, Nat. Phys. **6**, 645 (2010).

[57] P. Hirschfeld, M. Korshunov, and I. Mazin, Rep. Prog. Phys. **74**, 124508 (2011).

[58] G. R. Stewart, Rev. Mod. Phys. **83**, 1589 (2011).

[59] F. Wang and D.-H. Lee, Science **332**, 200 (2011).

[60] A. Chubukov, Annu. Rev. Condens. Matter Phys. **3**, 57 (2012).

[61] A. Chubukov and P. J. Hirschfeld, Phys. Today **68**, No. 6, 46 (2015).

[62] L. Fu and C. L. Kane, Phys. Rev. Lett. **100**, 096407 (2008).

[63] R. P. Day, M. Na, M. Zingl, B. Zwartsenberg, M. Michiardi, G. Levy, M. Schneider, D. Wong, P. Dosanjh, T. M. Pedersen, S. Gorovikov, S. Chi, R. Liang, W. N. Hardy, D. A. Bonn, S. Zhdanovich, I. S. Elfimov, and A. Damascelli, Phys. Rev. B **105**, 155142 (2022).

[64] E. J. König and P. Coleman, Phys. Rev. Lett. **122**, 207001 (2019).

[65] S. Qin, L.-H. Hu, C. Le, J. Zeng, F.-C. Zhang, C. Fang, and J. Hu, Phys. Rev. Lett. **123**, 027003 (2019).

[66] P. Hosur, P. Ghaemi, R. S. K. Mong, and A. Vishwanath, Phys. Rev. Lett. **107**, 097001 (2011).

[67] C.-K. Chiu, M. J. Gilbert, and T. L. Hughes, Phys. Rev. B **84**, 144507 (2011).

[68] C.-K. Chiu, P. Ghaemi, and T. L. Hughes, Phys. Rev. Lett. **109**, 237009 (2012).

[69] Z.-Z. Li, F.-C. Zhang, and Q.-H. Wang, Sci. Rep. **4**, 1 (2014).

[70] L.-H. Hu, C. Li, D.-H. Xu, Y. Zhou, and F.-C. Zhang, Phys. Rev. B **94**, 224501 (2016).
[71] Z. Yan, Z. Wu, and W. Huang, Phys. Rev. Lett. **124**, 257001 (2020).
[72] C.-K. Chiu, T. Machida, Y. Huang, T. Hanaguri, and F.-C. Zhang, Sci. Adv. **6**, eaay0443 (2020).
[73] A. Ghazaryan, P. L. S. Lopes, P. Hosur, M. J. Gilbert, and P. Ghaemi, Phys. Rev. B **101**, 020504(R) (2020).
[74] C. Li, X.-J. Luo, L. Chen, D. E. Liu, F.-C. Zhang, and X. Liu, arXiv:2107.11562.
[75] S. Qin, L.-H. Hu, X. Wu, X. Dai, C. Fang, F.-C. Zhang, and J. Hu, Sci. Bull. **64**, 1207 (2019).
[76] S. Borisenko, D. Evtushinsky, Z.-H. Liu, I. Morozov, R. Kappenberger, S. Wurmehl, B. Buchner, A. Yaresko, T. Kim, M. Hoesch *et al.*, Nat. Phys. **12**, 311 (2016).
[77] H. Zhang, C.-X. Liu, X.-L. Qi, X. Dai, Z. Fang, and S.-C. Zhang, Nat. Phys. **5**, 438 (2009).
[78] C.-X. Liu, X.-L. Qi, H. J. Zhang, X. Dai, Z. Fang, and S. C. Zhang, Phys. Rev. B **82**, 045122 (2010).
[79] N. P. Armitage, E. J. Mele, and A. Vishwanath, Rev. Mod. Phys. **90**, 015001 (2018).
[80] B. Q. Lv, T. Qian, and H. Ding, Rev. Mod. Phys. **93**, 025002 (2021).
[81] Most bulk iron-based superconductors, including these TFeSC candiddates focused in this Letter, are commonly believed to carry an $s_{\pm}$-wave pairing symmetry [82]. Since the $s_{\pm}$-wave pairing will contribute to the vortex topology in the same way as an isotropic s-wave pairing, we choose to use the s-wave pairing in our model for simpliciy.
[82] P. J. Hirschfeld, M. M. Korshunov, and I. I. Mazin, Rep. Prog. Phys. **74**, 124508 (2011).
[83] C.-K. Chiu, J. C. Y. Teo, A. P. Schnyder, and S. Ryu, Rev. Mod. Phys. **88**, 035005 (2016).
[84] See Supplemental Material at http://link.aps.org/supplemental/10.1103/PhysRevLett.129.277001 for numerical details on the vortex spectrum calculations, analytical analysis on how the DSM bands will renormalize the TI bands in the infinite δ_{so} limit, the low-energy projection for the effective vortex Hamiltonians, the C_4-breaking vortex Hamiltonian by tilting magnetic field, the effect of curved vortex line induced by bulk impurities, and a discussion of vortex topological phase diagram for $CaKFe_4As_4$, which includes Refs. [33,65,66,85–92].
[85] S. S. Zhang, J.-X. Yin, G. Dai, H. Zheng, G. Chang, I. Belopolski, X. Wang, H. Lin, Z. Wang, C. Jin, and M. Z. Hasan, Phys. Rev. B **99**, 161103(R) (2019).
[86] C. Li, L.-H. Hu, and F.-C. Zhang, Sci. China Phys. Mech. Astron. **62**, 1 (2019).
[87] E. H. Brandt, Rep. Prog. Phys. **58**, 1465 (1995).
[88] A. Kitaev, in *AIP Conference Proceedings* (American Institute of Physics, New York, 2009), Vol. 1134, pp. 22–30.
[89] S. Ryu, A. P. Schnyder, A. Furusaki, and A. W. Ludwig, New J. Phys. **12**, 065010 (2010).
[90] C. Fang, M. J. Gilbert, and B. A. Bernevig, Phys. Rev. Lett. **112**, 106401 (2014).
[91] X.-J. Liu, J. J. He, and K. T. Law, Phys. Rev. B **90**, 235141 (2014).
[92] S. Kobayashi and A. Furusaki, Phys. Rev. B **102**, 180505(R) (2020).
[93] M. Cheng and H.-H. Tu, Phys. Rev. B **84**, 094503 (2011).
[94] R.-X. Zhang and C.-X. Liu, Phys. Rev. Lett. **120**, 156802 (2018).
[95] F. Gygi and M. Schlüter, Phys. Rev. B **43**, 7609 (1991).
[96] R. Giwa and P. Hosur, Phys. Rev. Lett. **127**, 187002 (2021).
[97] R. Giwa and P. Hosur, arXiv:2203.06893.
[98] M. Li, G. Li, L. Cao, X. Zhou, X. Wang, C. Jin, C.-K. Chiu, S. J. Pennycook, Z. Wang, and H.-J. Gao, Nature (London) **606**, 890 (2022).
[99] W. Liu, Q. Hu, X. Wang, Y. Zhong, F. Yang, L. Kong, L. Cao, G. Li, K. Okazaki, T. Kondo *et al.*, arXiv:2111.03786.